Supporting Information

Influence of Surfactant on Crystallization Kinetics of Stearic Acid

*Hiya Goswami and Jyoti R. Seth**

Department of Chemical Engineering, Indian Institute of Technology Bombay, Powai, Mumbai-400076, India.

*jyoti@che.iitb.ac.in, Tel: +91 (22) 2576 7226 Fax: +91 (22) 2572 6895

SOLUBILITY OF SA IN MO

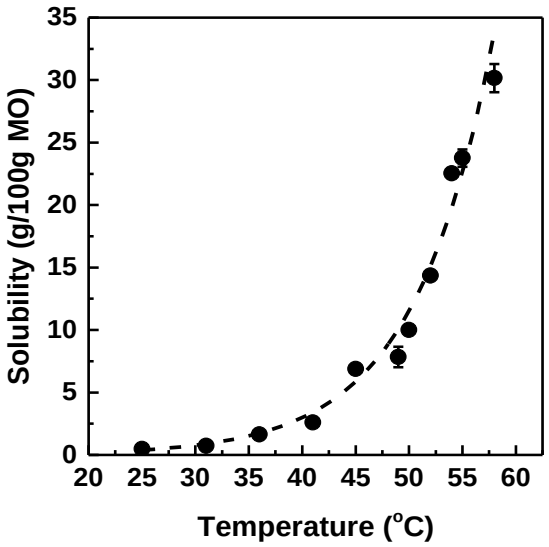

Figure S1 Solubility of SA in MO as a function of temperature.

At room temperature (25 ℃), the solubility of SA in MO is $C_{SA}^{0} = 0.4\%$. Figure S1 represents the solubility of SA in MO at different temperatures. The solubility of SA in MO at 25 ^{o}C was also verified by turbidity measurements.

In the presence of Span 80, the solubility of SA in MO at 25 ^{o}C was determined using turbidity measurements. By extrapolating the solubility data for different surfactant concentrations, it was found that there is negligible change in solubility of SA for up to 0.08 wt. % surfactant.

MORPHOLOGY OF C-FORM CRYSTAL OF SA

For C-form, the crystal is lozenge shaped with an acute angle of 55°. Figure S2 is a schematic of the same. Distance between the two farthest endpoints is termed as the major axis (L_1). The distance between the other two endpoints is marked as the minor axis (L_2). The estimated ratio of L_1 to L_2 should be 1.96.

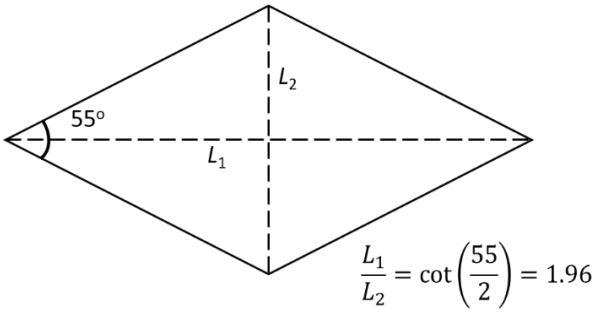

Figure S2 Schematic of C-form crystal of SA.

INFLUENCE OF SURFACTANT ON SELECTION OF POLYMORPHS

XRD measurements were performed on a Panalytical, Empyrean powder X-ray diffractometer to determine the polymorphic forms of filtered SA crystals, crystallized with and without surfactant. The diffractometer is equipped with a CuKα source (λ=1.54 Å) and was operated to record wide-angle XRD patterns in the 2θ range from 5º to 15º with a step-size of 1º/min.

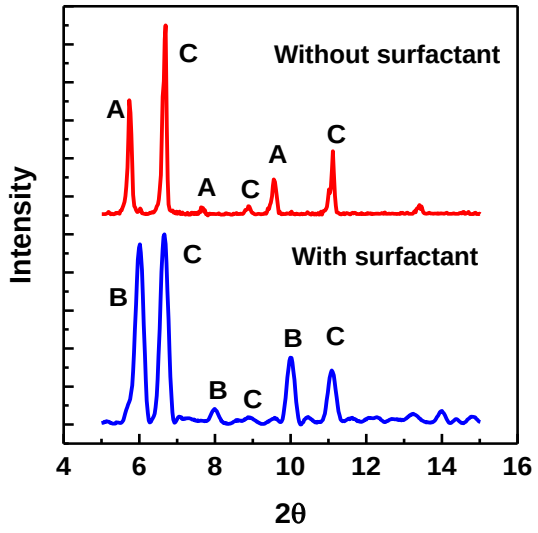

Figure S3 XRD patterns of SA crystallized without (top) and with (bottom) surfactant in MO. A- and C-forms were observed without surfactant (σ_0 = 2, quiescent cooling) and B- and C-forms were observed with surfactant (σ_0 = 2, $C_{\text{surf}} = 0.07\%$, quiescent cooling). The positions were confirmed by comparison with literature.[25,36]

REPRESENTATIVE IMAGES AT DIFFERENT SUPERSATURATIONS

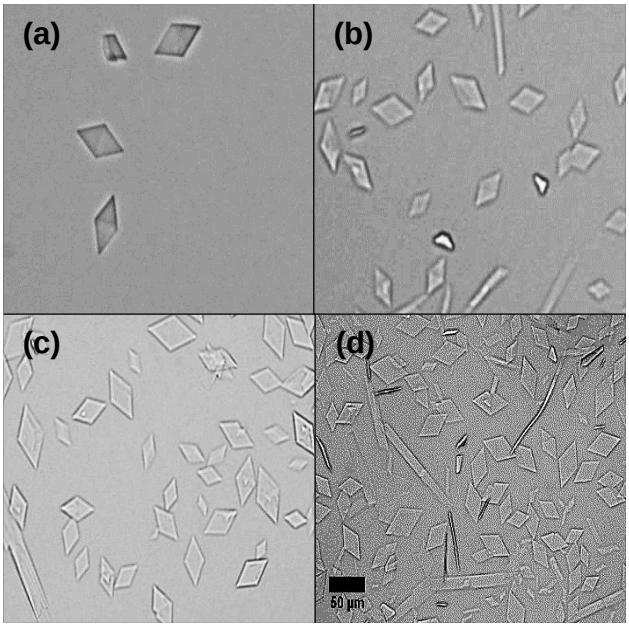

Figure S4 Bright-field micrographs at different relative supersaturations, σ_0 = (a) 0.5, (b) 1, (c) 1.5 and (d) 2. Increase in number of crystals as a function of relative supersaturation, σ_0, is seen in these images. The optical micrographs were recorded at around 30 min from the time of induction.

VISCOSITY OF MO WITH DIFFERENT SURFACTANT CONCENTRATIONS

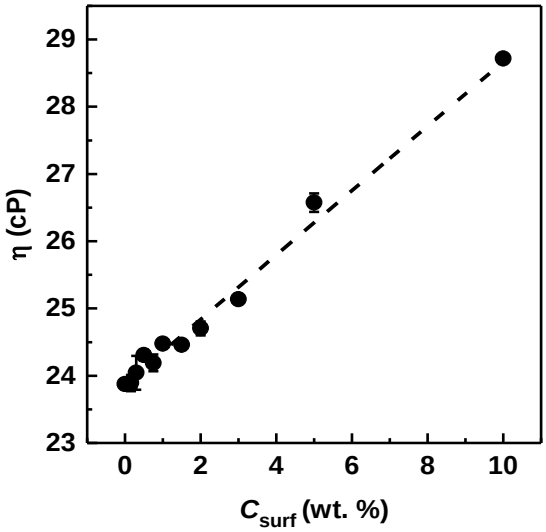

Figure S5 Plot of viscosity of MO with different surfactant concentrations. The dashed line is a linear fit.

Solutions of Span 80 in MO with concentrations ranging from (0.1-10 wt. %) were made. Viscosity of these solutions was measured in an MCR 301 Anton Paar Rheometer. Viscosity increases linearly with surfactant concentration with no indication of micelle formation.

Further, the same solutions were tested for scattering by DLS (Zetasizer, nano ZS, Malvern). No appreciable scatter was observed. This again confirmed that there was no micellar formation due to Span 80 in MO within the range of concentration of interest.

REPRESENTATIVE IMAGES AT DIFFERENT SURFACTANT CONCENTRATIONS

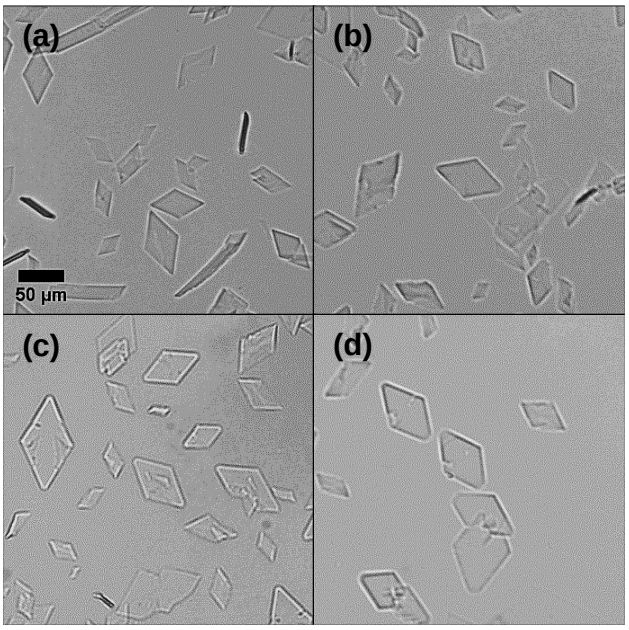

Figure S6 Bright-field micrographs of SA crystals at relative supersaturation, σ_0 = 2, with varying C_{surf} (a) 0.05, (b) 0.06, (c) 0.07 and (d) 0.08%. The optical micrographs were recorded at around 30 min from the time of induction.

Change in crystal morphology with increasing surfactant concentration is represented above. Aspect ratio of the crystals decreased with increasing surfactant concentration.

THICKNESS OF CRYSTALS CALCULATED FOR DIFFERENT RELATIVE SUPERSATURATIONS AND SURFACTANT CONCENTRATIONS

In these experiments, a 10 μl of solution was added on a glass slide and a coverslip was immediately placed over it. The amount of SA crystallized for this volume was estimated from the solubility data. The solution would spread evenly over the entire coverslip area, A = 4.84×10^{-4} m^2. The fraction of area covered by SA crystals is calculated from the number of crystals and their average size. The density of SA is 1.018 g/cm^3 and that of MO is 0.845 g/cm^3 at 25 ^oC. Thus, the thickness, *h* can be calculated as

$$h = \frac{g\ of\ SA\ crystallised\ in\ 10\ \mu l\ solution}{Density\ of\ SA\ \times\ area\ covered\ by\ SA\ crystals} \quad (1)$$

Table S1. Estimated thicknesses at different relative supersaturations, σ_0.

Relative supersaturation, σ_0	% area covered by crystals of the entire crystallizing area, A	Thickness (μm)
0.5	5.0	0.7
1	18.0	0.4
1.5	40.0	0.3
2	70.0	0.2
2.5	85.0	0.2

Table S2. Estimated thicknesses for $\sigma_0 = 1$ at varying C_{surf} (wt. %).

C_{surf} (wt. %)	% area covered by crystals of the entire crystallizing area, A	Thickness (μm)
0.03	18.0	0.4
0.04	16.0	0.4
0.05	14.0	0.5
0.06	12.0	0.6

COMPARISON BETWEEN PREDICTED AND FITTED VALUES OF MAXIMUM CRYSTAL SIZE AND THE TIME SCALE OF GROWTH FOR DIFFERENT RELATIVE SUPERSATURATIONS

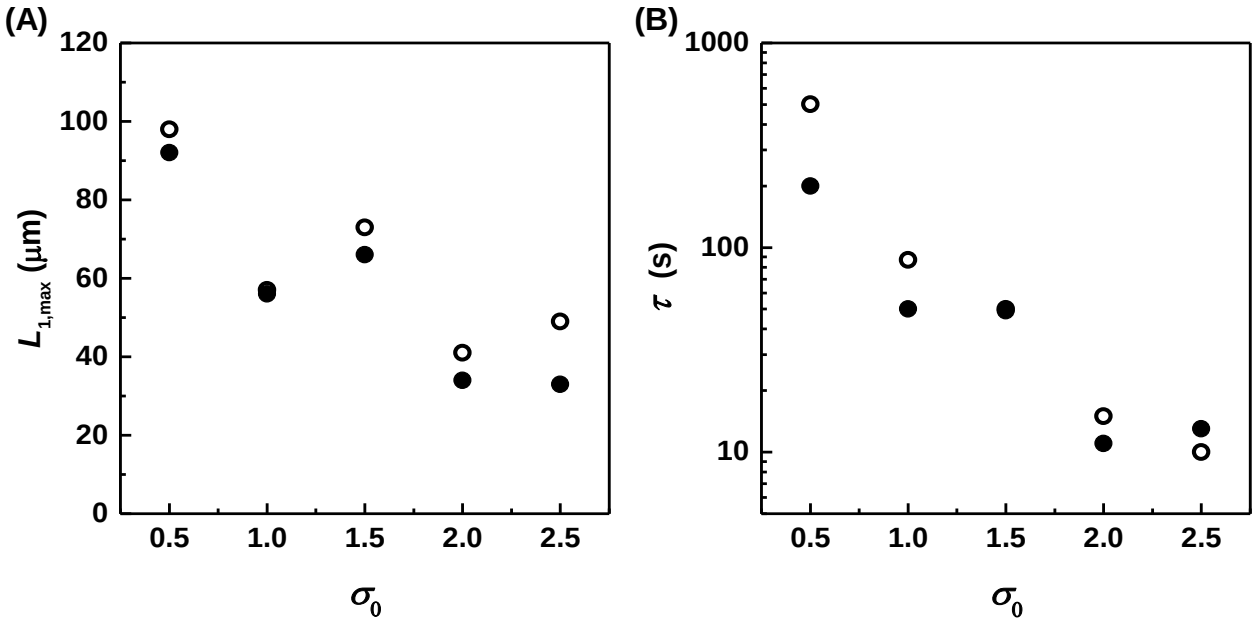

Figure S7 Predicted (o) and fitted values (●) of (A) $L_{1,max}$, and (B) τ, for different relative supersaturations, σ_0. The fitted values are obtained by using eq 10 to fit the data for L_1 and L_2 versus time for different supersaturations.

EFFECT OF SURFACTANT ON GROWTH RATES

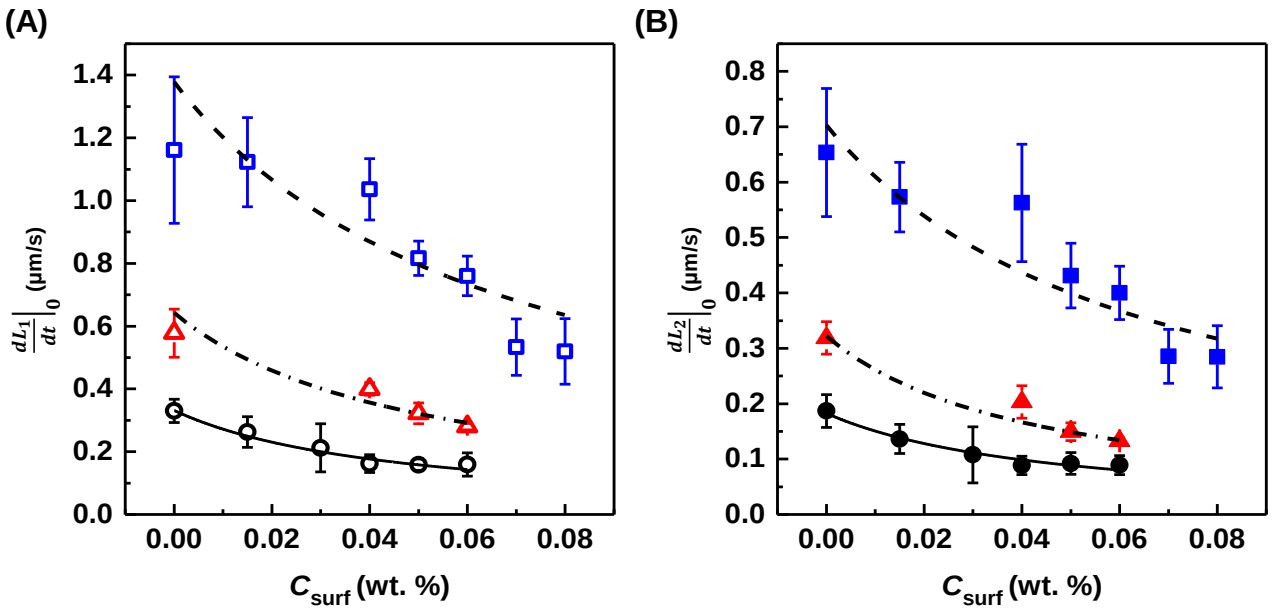

Figure S8 Initial growth rates for major (open symbols) and minor axes (filled symbols) versus C_{surf}. Data for different supersaturations [σ_0 = 1(o,●), 1.5 (△,▲) and 2 (□,■)]. Lines are best fits using eq 7.

CRYSTAL GROWTH MECHANISM

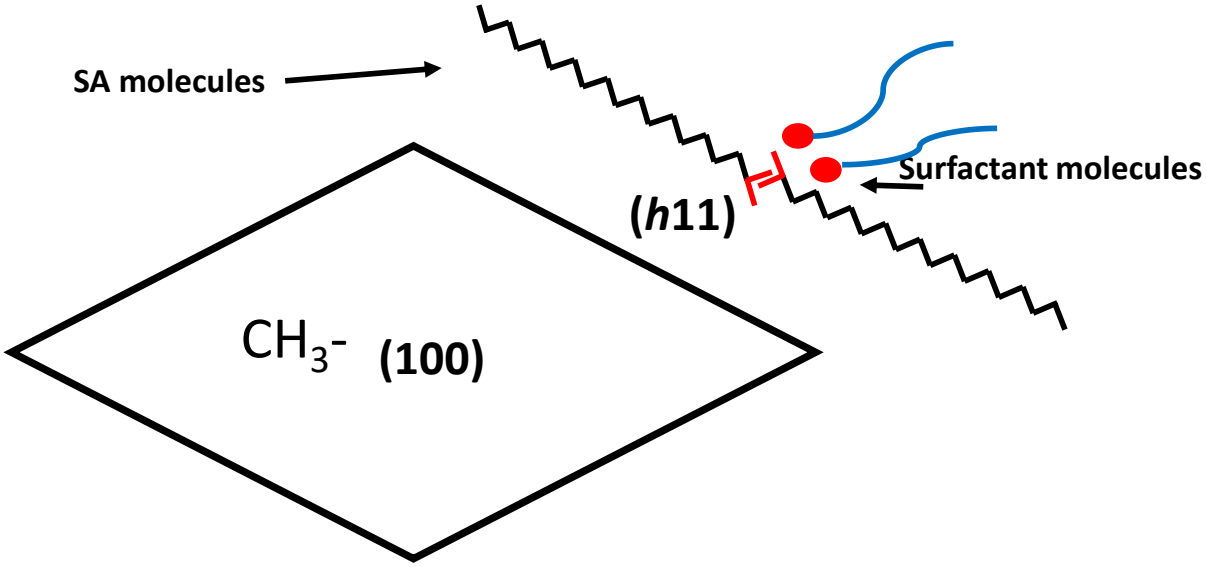

Figure S9 Schematic of the interaction between SA and Span 80 molecules during crystal growth.

EVIDENCE OF SECONDARY NUCLEATION

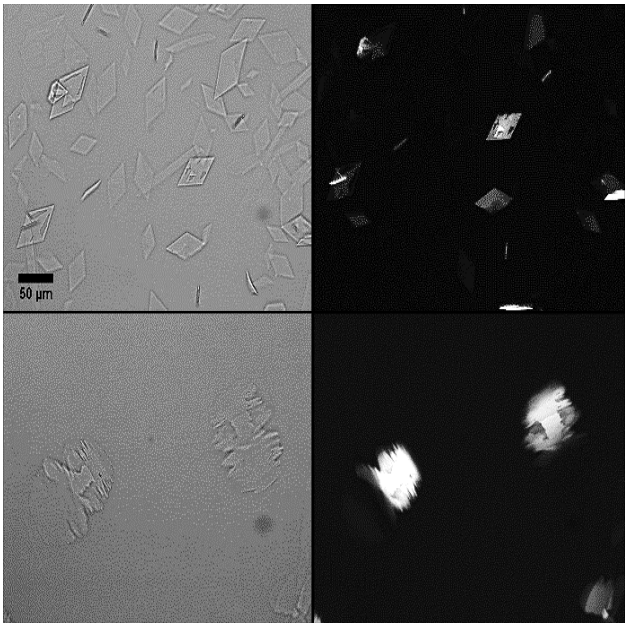

Figure S10 Bright-field (left) and corresponding cross-polarized light (right) images of SA crystals at σ_0 = 2, without (top) and with 0.08 wt.% surfactant (bottom). Secondary nucleation is seen as the bright surface patches in the cross polarised light images, observed in the presence of surfactant.